AJChE 2017, Vol. 17, No. 1, 46 – 61

Polyamide Chain Growth and Crosslinking: The Controlling Determinants for Properties of Thin Film Composite Membrane

J.J. Beh [*,1]
E.P. Ng [2]
B.S. Ooi [1]
[1] *School of Chemical Engineering, Engineering Campus, Universiti Sains Malaysia, Seri Ampangan, 14300 Nibong Tebal, Pulau Pinang, Malaysia*
[2] *School of Chemical Sciences, 11800 Universiti Sains Malaysia, Pulau Pinang, Malaysia*
[*]*e-mail:* bjj14_kkk021@student.usm.my

The desired features of a polyamide thin film composite (TFC) membrane for desalination can be tailored through careful control of membrane preparation condition. This work aims to provide more comprehensive understanding on polyamide film formation chemistry in order to correlate the membrane synthesis condition with its characteristics. Three series of TFC membranes were prepared by interfacial polymerization with adjustment of m-phenylenediamine (MPD) and trimesoyl chloride (TMC) monomer concentration as well as reaction duration. The membrane structural properties were evaluated based on glucose permeation then correlated with the transport and charge behaviors of membrane determined from pure water and inorganic salt permeation. During interfacial polymerization, competition occurs between polyamide chain growth and crosslinking. It was found that higher MPD concentration promoted polyamide chain crosslinking while increasing TMC concentration favored polyamide chain growth during diffusion-limited growth stage. Meanwhile, prolonged degree of polyamide chain growth and crosslinking occurred at longer reaction duration, which eventually caused self-limiting membrane growth. The water transport was primarily controlled by polyamide film thickness, porosity and hydrophilicity while size exclusion and Donnan exclusion worked in tandem in governing the salt separation. The TFC membrane synthesized at 3 w/v% MPD concentration and 0.10 w/v% TMC concentration under 60 s reaction duration achieved the best desalination performance with pure water permeability of 0.853 L/m^2·h·bar and 81.4 % NaCl rejection.

Keywords : Thin film composite membrane; Interfacial polymerization; Monomer concentration; Reaction duration; Chain growth; Chain crosslinking

INTRODUCTION

In 1970s, a significant breakthrough was discovered in membrane technology for desalination with the pioneering development of thin film composite (TFC) membrane (Cadotte et al. 1972). TFC membrane is produced from interfacial polymerization between amine monomer in aqueous solution and acid chloride

monomer in organic solution. The most common monomer choice for TFC membrane synthesis is m-phenylenediamine (MPD) and trimesoyl chloride (TMC) (Tomaschke 2000). MPD is a bifunctional amine (-NH_2) capable of yielding TFC membrane with very high salt rejection (Tomaschke 2000). Meanwhile, TMC is a trifunctional acid chloride (-COCl) which endows the TFC membrane with crosslinking sites by virtue of having one extra functional group than MPD for crosslinking reaction with MPD. The reaction between MPD and TMC results in a thin and dense polyamide film. The transport and separation performance of TFC membrane is dictated by the polyamide film morphology and properties, which can be fully understood with insight on interfacial polymerization chemistry.

Generally, interfacial polymerization involves two competing reactions: polyamide chain growth and crosslinking. It is a highly non-linear process best described by a multistage membrane formation mechanism (Song et al. 2005). The whole reaction can be generalized into two stages, namely incipient film formation and the subsequent diffusion-limited growth (El-Aassar 2012, Freger 2005, Hermans et al. 2015). The incipient film formation is an instantaneous process dominated by polyamide chain growth at the onset of reaction. Here, MPD and TMC react with each other at the liquid-liquid interface to quickly form a relatively thin and dense polyamide film. Then, the diffusion-limited growth takes over where the polyamide chain crosslinking becomes more prominent and competes with polyamide chain growth. Since the reactions occur predominantly in organic solution due to exceptionally low TMC solubility in aqueous solution (Chai et al. 1994, Tomaschke 2000), MPD needs to partition into the organic solution then diffuses across the incipient polyamide film for further membrane growth. The incipient polyamide film represents an additional barrier for MPD diffusion into the reaction zone. Consequently, self-limiting phenomenon occurs where the membrane growth is gradually retarded and eventually ceases when MPD is unable to penetrate through the polyamide film (Freger 2005, Hermans et al. 2015, Song et al. 2005). Hence, membrane formation depends not only on the reaction but also on MPD transport into the polyamide film (Atherton 1994). Since interfacial polymerization is a very quick reaction, the overall film formation rate is primarily governed by MPD diffusion rate (Rudin et al. 2012, Tomaschke 2000).

Many past researches have shown that the TFC membrane structure and features are strongly correlated with membrane preparation condition (Freger 2005, Petersen 1993, Soroush et al. 2012). However, most of them often relate membrane synthesis parameter directly with its final properties without describing how polyamide film structure evolves over time to arrive at the final membrane morphology. The understanding on polyamide film formation mechanism is essentially critical as it allows the conceptualization of membrane structure at various stages of reaction instead of at the end of reaction only. This importance is highlighted by the work of Hermans et

al., who revealed that the TFC membrane performance is primarily governed by the incipient polyamide film (Hermans et al. 2015). Since this layer is formed instantaneously during reaction, accurate characterization is nearly impossible so its structure can only be theorized through polyamide film formation principle. Besides, without this knowledge, it is hard to explicate previous works with contradicting results on the study of same synthesis variable. For instance, both Roh et al. and Lee et al. studied TMC concentration during membrane synthesis but obtained different final membrane structure and performance (Lee et al. 2013, Roh et al. 2006). While Lee et al. attributed their result to the absence of support layer during membrane development (Lee et al. 2013), it is not clear how their polyamide film formation process differs from the work of Roh et al. to cause the contrasting final membrane morphology.

In view of the limitations exposed by previous works, this study aims to contribute more detailed understanding on interfacial polymerization chemistry in order to provide insight on how the polyamide film evolves into its final morphology and properties during membrane development. The concentration of monomers and reaction duration have been singled out as the membrane synthesis parameters for study as they control the rate and extent of reaction respectively, in which a proper balance is necessary to obtain the desired TFC membrane features for desalination. In this work, the transport and charge behaviors of TFC membrane were evaluated via pure water and inorganic salt permeation. These were then correlated with the structural properties of TFC membrane determined from Hagen-Poiseuille equation and Donnan steric pore model (DSPM) based on glucose permeation. This method was chosen as it has been proven to provide good accuracy in correlating structural properties with separation performance of TFC membrane (Bowen et al. 1996). For each adjustment of membrane synthesis parameter, the polyamide film formation was conceptualized throughout the whole reaction duration to better apprehend the development of TFC membrane structure and properties.

EXPERIMENT

Preparation of Polysulfone Support Membrane

15 wt% polysulfone Udel P-1700 (PSf, Solvay Advanced Polymer, L.L.C.) and 18 wt% polyvinylpyrrolidone (PVP-10, Sigma Aldrich) were dissolved in N-methylpyrrolidone (NMP, Merck) then homogenized for 24 h. The PSf solution was degassed and cast onto a non-woven polyester fabric (Texlon Corporation) firmly attached on a glass plate at thickness of 150 μm. The glass plate was instantly immersed into the distilled water bath at room temperature to allow complete PVP and NMP solvent removal. After 24 h, the PSf support membrane was harvested.

Synthesis of Thin Film Composite (TFC) Membrane

Three series of TFC membranes were synthesized from interfacial

polymerization between MPD (Merck) and TMC (Sigma Aldrich), which were dissolved in deionized water (Milli-Q) and n-hexane (Merck) respectively. The concentration of both monomers and reaction duration were systematically adjusted according to **Table 1**. Firstly, the PSf support membrane was fixed onto a flat Teflon chamber plate and MPD solution was poured onto the support. After 10 min, excess MPD solution was removed from the membrane surface using a rubber roller. The membrane was then immersed with TMC solution for a predetermined reaction duration. The membrane underwent heat curing treatment at 60 ◦C for 15 min before being dried in air to ensure the firm attachment of polyamide film onto the support membrane.

Table 1. TFC membrane preparation condition.

Series	MPD concentration (w/v%)	TMC concentration (w/v%)	Reaction duration (s)
1	1-3	0.10	60
2	2	0.05-0.15	60
3	2	0.10	30-90

Properties Characterization of TFC Membrane

Pure water, inorganic salt and glucose permeation tests were carried out on the synthesized TFC membranes. Membrane transport equations were used to translate their performance into membrane structural and transport properties. In order to enhance the permeation flux, each TFC membrane was prewetted before the permeation test by immersing the membrane into deionized water for 10 min followed by aqueous solution of 30 v/v% ethanol (Merck). After 24 h, the membrane was transferred back into deionized water for 10 min then immediately used for filtration experiment.

The permeation test was conducted at room temperature with a dead end stirred cell (Sterlitech HP4750) having effective membrane area of 14.6 cm^2. Prior to filtration test, each TFC membrane was compressed with nitrogen gas (Well Gas) at 8 bar for 1 h. All experiments were performed under 350 rpm stirring speed and allowed for 30 min of process equilibration before data collection commenced.

Pure water permeation was carried out with 18.2 MΩ·cm deionized water (Milli-Q) at pressure of 3-7 bar. The flux was calculated using Eq. (1). Pure water permeability was determined from the linear fitting of flux and transmembrane pressure data based on Eq. (2).

$$J_w = \frac{\Delta V}{A_m \cdot \Delta t} \quad (1)$$

$$J_w = A\Delta P \quad (2)$$

Where J_w is pure water flux, ΔV is permeate volume, A_m is effective membrane area, Δt is time, A is pure water permeability and ΔP is transmembrane pressure.

Inorganic salt permeation was conducted at pressure of 7 bar with aqueous solutions of sodium chloride (NaCl, Merck), sodium sulfate (Na_2SO_4, Merck), magnesium chloride ($MgCl_2$, Merck) and magnesium sulfate ($MgSO_4$, Merck) at 10 mM feed concentration. The

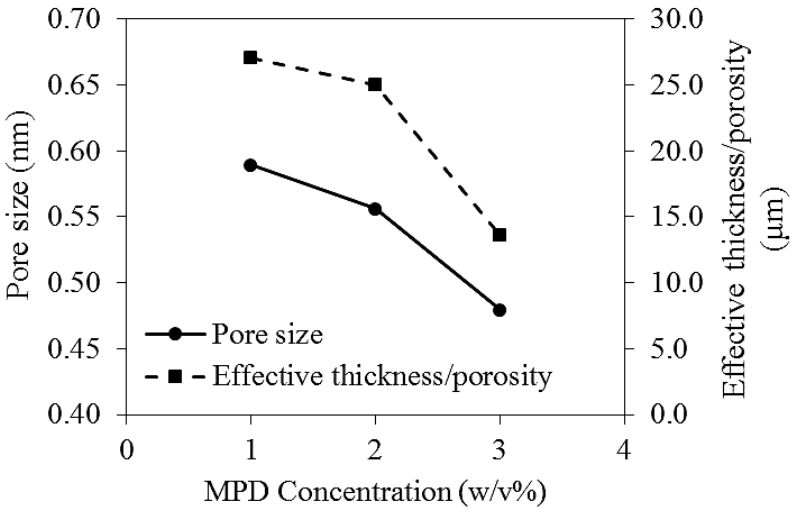

Fig. 1: Structural Properties of TFC Membrane at Varying MPD Concentration.

salt rejection was evaluated using Eq. (3). Both feed and permeate salt concentrations were analyzed using a conductivity meter (Starter 300C, Ohaus). The bulk feed concentration was averaged from the initial and final feed concentration while the permeate concentration was averaged from two permeate concentration readings. The salt permeability was further determined based on solution-diffusion theory using Eq. (4). The solution osmotic pressure was estimated using van't Hoff's equation for dilute solution according to Eq. (5).

$$R_s = 1 - \frac{C_p}{C_f} \tag{3}$$

$$B = A(\Delta P - \Delta\pi)\left(\frac{1 - R_s}{R_s}\right) \tag{4}$$

$$\pi = nCRT \tag{5}$$

Where R_s is salt rejection, C_p is permeate concentration, C_f is bulk feed concentration, B is salt permeability, $\Delta\pi$ is osmotic pressure difference, n is van't Hoff's factor (dissociation degree of solute), C is solute concentration, R is universal gas constant and T is solution temperature.

The permeation for aqueous solution of glucose (Merck) was performed at pressure of 3-7 bar with feed concentration of 300 ppm. The flux and rejection were determined in a similar fashion to Eq. (1) and Eq. (3) respectively. The data were then fitted with Hagen-Poiseuille equation and DSPM using SigmaPlot 12 (Systat Software Inc.) to obtain the structural properties of TFC membrane (pore size and effective thickness/porosity). The fundamental and governing equations of DSPM are described elsewhere (Bowen et al. 1997).

RESULTS AND DISCUSSIONS

Properties of TFC Membrane at Varying MPD Concentration

The first series of TFC membrane was synthesized with MPD concentration ranging from 1 to 3 w/v%. **Figure 1** shows

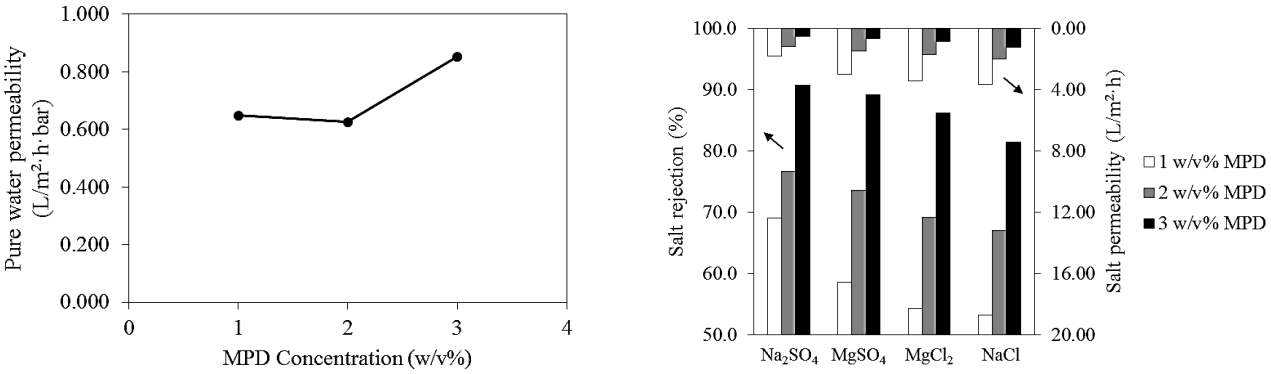

(a) (b)

Fig. 2: Transport Properties of TFC Membrane at Varying MPD Concentration for (a) Pure Water (b) Inorganic Salts

that increasing MPD concentration gradually reduced membrane pore size with greater drop at higher MPD concentration (5.6 % from 1 to 2 w/v% and 13.8 % from 2 to 3 w/v%). The membrane effective thickness/porosity also followed similar decreasing trend (7.7 % from 1 to 2 w/v% and 45.5 % from 2 to 3 w/v%). This could be explained by the conceptualization of polyamide film formation process. At the onset of reaction, there was minimum MPD diffusion resistance so the overall reaction was rate-controlled by concentration of TMC, which was the limiting reactant. Since this series of membrane was synthesized from the same TMC concentration, the incipient polyamide film formed immediately with undistinguishable feature between different MPD concentrations. Hence, the membrane final structure was derived from the subsequent diffusion-limited growth stage.

During this stage, MPD diffusion into polyamide film began to exert influence on polyamide film formation. By Fick's law of diffusion, higher MPD concentration improved MPD diffusion rate into polyamide film (Fick 1855). This greatly enhanced the polyamide chain crosslinking as the -COCl crosslinking sites were highly likely to be reacted with more MPD in polyamide film. Hence, the polyamide film tightened up to result in smaller membrane pore. Lower membrane porosity should then follow sensibly but the decreasing membrane effective thickness/porosity implied that greater degree of polyamide film thickness reduction occurred at higher MPD concentration. This was attributed to the stronger MPD transport hindrance across polyamide film by the smaller pore, which further increased the likeliness of polyamide chain crosslinking. Consequently, the polyamide film thickness growth became more restricted at higher MPD concentration. The more significant structural change from 2 to 3 w/v% MPD concentration indicated that polyamide chain growth was severely retarded by extensive polyamide chain crosslinking at 3 w/v% MPD concentration to result in a very thin polyamide film.

Figure 2 illustrates the transport properties of TFC membrane at increasing MPD concentration. From Figure 2 (a), the

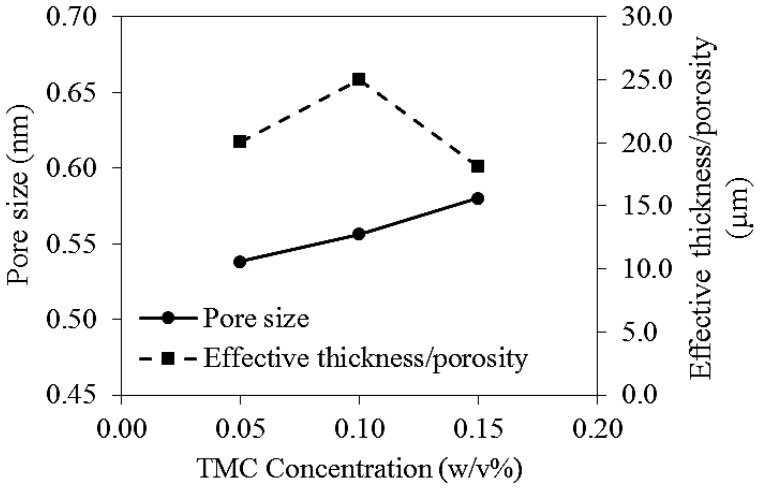

Fig. 3: Structural properties of TFC membrane at varying TMC concentration

pure water permeability was essentially similar at 1 and 2 w/v% MPD concentration before increased greatly by 36.3 % at 3 w/v% MPD concentration. As MPD concentration increased from 1 to 2 w/v%, the membrane pore size and porosity reduced, which theoretically produces a membrane with poor pure water permeability. However, this was offset by the formation of a thinner membrane, which principally favors water transport. Hence, the combined effects resulted in the plateau of pure water permeability at 1 and 2 w/v% MPD concentration. While similar membrane structural change occurred at 3 w/v% MPD concentration, the corresponding polyamide film was very thin thus overcame the membrane pore size and porosity reduction to induce the pure water permeability rise at 3 w/v% MPD concentration.

Meanwhile, the salt rejection improved by a big margin from 1 to 3 w/v% MPD concentration as shown in Figure 2 (b). The enhancement of salt rejection at higher MPD concentration was the consequence of membrane morphology change as the trend was salt-independent. As the membrane pore reduced in size from 1 to 3 w/v% MPD concentration, the molecular sieving effect of membrane was heightened thus leading to much improved salt rejection. The membrane selectivity was not even affected by the high pure water permeability at 3 w/v% MPD concentration as the enhanced size exclusion effect reduced the salt concentration inside polyamide film to minimize the contribution of convective salt transport. With such significant rise in salt rejection, it was not surprising that salt permeability dropped at higher MPD concentration.

Properties of TFC Membrane at Varying TMC Concentration

The second series of TFC membrane was synthesized by adjusting TMC concentration from 0.05 to 0.15 w/v%. The structural properties of TFC membrane are depicted in **Figure 3**. The membrane pore size gradually rose by 7.8 % from 0.05 to 0.15 w/v% TMC concentration. However,

the membrane effective thickness/porosity first increased by 24.4 % from 0.05 to 0.10 w/v% TMC concentration before suffered 27.5 % drop at 0.15 w/v% TMC concentration. This membrane morphology change could be elucidated by the role of TMC in interfacial polymerization. Principally, TMC has certain degree of influence on reaction rate (Ahmad et al. 2005), particularly during incipient film formation where there is minimum MPD diffusion barrier. With higher reaction rate at increasing TMC concentration and domination of polyamide chain growth at the onset of reaction, the incipient polyamide film formed from higher TMC concentration was thicker. This thickness difference had a propagating effect on the subsequent diffusion-limited growth stage.

The incipient polyamide film at 0.05 w/v% TMC concentration was the thinnest with the lowest MPD diffusion resistance but it also had the least -COCl crosslinking sites due to low polyamide chain growth rate. The relative -COCl deficiency compared to MPD ensured that most crosslinking sites were reacted by the incoming MPD. As a result, the membrane experienced pore tightening to restrict the MPD transport across polyamide film. This combined with the low TMC concentration to limit polyamide chain growth. Hence, the polyamide film formed was thin but well crosslinked.

For 0.10 w/v% TMC concentration, the incipient polyamide film was thicker. With presence of more -COCl crosslinking sites but similar MPD influx under the application of same MPD concentration, the crosslinking tendency of polyamide chain reduced. The subsequent MPD diffusion improvement under membrane pore loosening combined with the higher TMC concentration to enhance polyamide chain growth and film thickness significantly. Hence, the membrane effective thickness/porosity vastly increased at 0.10 w/v% TMC concentration. The theorized film thickness growth at higher TMC concentration was agreeable with past research findings (Ahmad et al. 2005, Lee et al. 2013, Roh et al. 2006).

Meanwhile, the incipient polyamide film at 0.15 w/v% TMC concentration was the thickest. There was insufficient MPD to react with the large number of -COCl crosslinking sites in polyamide film due to competition for MPD from enhanced polyamide chain growth at high TMC concentration. Besides, the polyamide chain crosslinking was further impeded by severe -COCl hydrolysis at high TMC concentration (Ahmad et al. 2005, Lee et al. 2013, Song et al. 2005). Thus, MPD diffused through the loose polyamide film easily for polyamide chain growth to induce film thickness increment. The membrane porosity was subsequently further enhanced by the region of thickness growth, which experienced limited polyamide chain crosslinking thus was relatively porous. This ultimately caused the membrane effective thickness/porosity to reduce at 0.15 w/v% TMC concentration in spite of the thickest polyamide film being formed.

Figure 4 displays the transport properties of TFC membrane at different TMC concentrations. A correlation was established between polyamide film

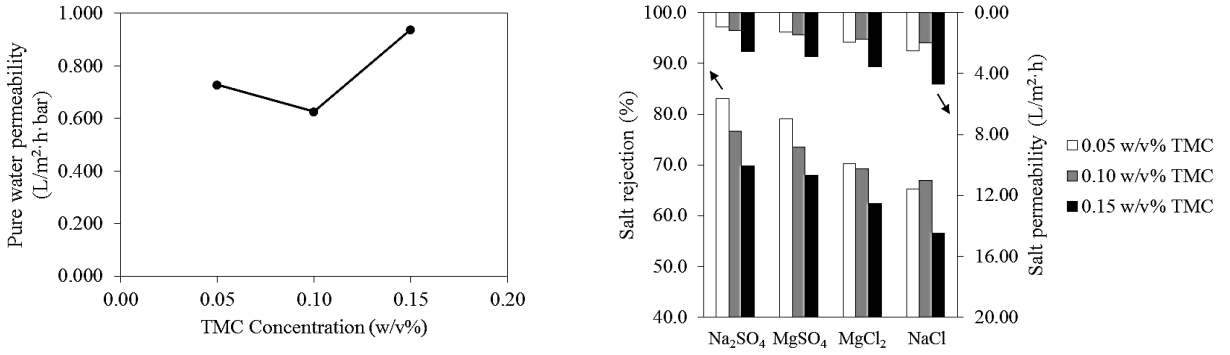

(a) (b)

Fig. 4: Transport properties of TFC membrane at varying TMC concentration for (a) pure water (b) inorganic salts

structure and its transport behavior. From Figure 4 (a), the pure water permeability decreased by 14.1 % from 0.05 to 0.10 w/v% TMC concentration but then increased by 49.9 % at 0.15 w/v% TMC concentration. Fundamentally, membrane pore loosening and film thickness increase contradict each other in impacting water transport. Such was the case for TMC concentration increment from 0.05 to 0.10 w/v%. At this rise of TMC concentration, the magnitude of membrane effective thickness/porosity increase (24.4 %) was substantially higher than the degree of membrane pore size increment (3.4 %). This implied that the negative effect of membrane thickness increase was more dominant thus negated the positive effect of membrane pore loosening to cause the drop of pure water permeability at 0.10 w/v% TMC concentration. However, severe -COCl hydrolysis occurred at 0.15 w/v% TMC concentration, which enhanced the membrane porosity and also hydrophilicity via enrichment by -COOH groups. These factors ultimately overcame the film thickness growth to enhance water transport as reflected by the highest pure water permeability at 0.15 w/v% TMC concentration.

Figure 4 (b) shows that the salt rejection gradually reduced from 0.05 to 0.15 w/v% TMC concentration. As the membrane pore was loosened up at increasing TMC concentration, its size exclusion effect was diminished. Hence, the polyamide film gradually lost its separation ability as indicated by the drop of salt rejection at higher TMC concentration. However, insignificant salt rejection difference was found at 0.05 and 0.10 w/v% TMC concentration for NaCl and $MgCl_2$. This suggested that other factor interfered with the size exclusion effect at these TMC concentrations. In essence, the separation of salt depends not only on size exclusion effect but also on Donnan exclusion effect, which achieves salt separation via interaction between membrane fixed electrical charges and ions (Yaroshchuk 2001). Donnan exclusion effect could not be neglected in this study as the membranes synthesized attained negative charges from the dissociation of -COOH groups into $-COO^-$ in aqueous environment. For a

negatively charged membrane, Donnan exclusion effect enhances the anion rejection via electrostatic repulsion between anion and membrane. Thus, in this study, the rejection of Cl^- and SO_4^{2-} ions was governed by both Donnan exclusion effect and size exclusion effect.

By Donnan exclusion principle, the SO_4^{2-} ion is rejected better than the Cl^- ion by a negatively charged membrane owing to its higher ionic valence. This effect is even more prevalent in a thinner membrane where the ionic membrane permeability is enhanced by the low membrane thickness (Yaroshchuk 2001). Such a case occurred for the polyamide film synthesized from 0.05 w/v% TMC concentration, where its low thickness amplified the weaker Donnan exclusion effect of Cl^- ion to impair its rejection. This counteracted the stronger size exclusion effect induced by smaller membrane pore at 0.05 w/v% TMC concentration. Hence, no rejection improvement was observed for NaCl and $MgCl_2$ when TMC concentration was reduced from 0.10 to 0.05 w/v%.

Meanwhile, the salt permeability trend varied with different salts from 0.05 to 0.10 w/v% TMC concentration (slight increase for SO_4^{2-} containing salts but slight decrease for Cl^- containing salts). Theoretically, salt permeability should rise at lower salt rejection as long as there is no substantial pure water permeability change to affect convective salt transport. Such a case occurred for Na_2SO_4 and $MgSO_4$. However, as NaCl and $MgCl_2$ exhibited similar rejection at 0.05 and 0.10 w/v% TMC concentration, the pure water permeability drop at 0.10 w/v% TMC concentration minimized the contribution of convective salt transport to reduce their permeabilities at this TMC concentration. Nevertheless, the salt permeability escalated by almost two-fold for all salts at 0.15 w/v% TMC concentration owing to the combined effects of membrane pore loosening and enhanced convective salt transport at this TMC concentration.

Properties of TFC Membrane at Varying Reaction Duration

The TFC membranes were synthesized at different reaction durations to investigate the temporal evolution of polyamide film structure. In essence, reaction duration defines the extent of reaction where prolonged degree of both polyamide chain crosslinking and growth occur at longer reaction time. Nevertheless, the reaction duration has a strong influence on the membrane structure, which can indirectly enhance or impede either reactions during membrane formation. The structural evolution of polyamide film is depicted in **Figure 5**. The membrane pore size declined gradually from 30 to 90 s. In the meantime, the membrane effective thickness/porosity remained similar at 30 and 60 s then dropped slightly at 90 s. Since the reaction duration in this study was much longer than the time for incipient film formation, the diffusion-limited growth stage ultimately defined the polyamide film structure.

The diffusion-limited growth stage started with a thin and loose incipient polyamide film owing to limited polyamide chain crosslinking. MPD could easily diffuse through the polyamide film

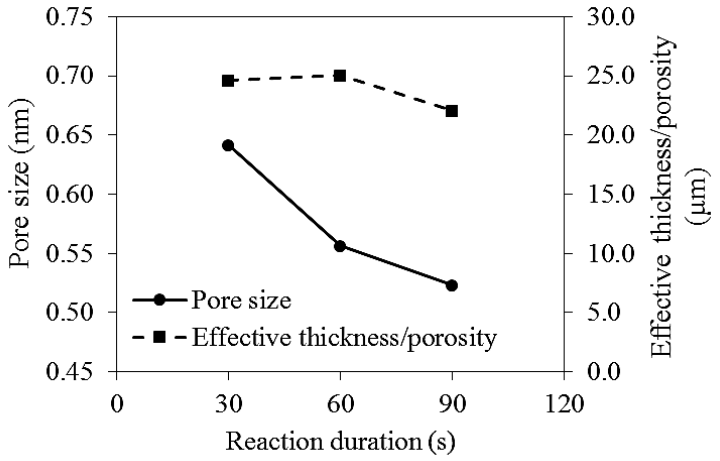

Fig. 5: Structural properties of TFC membrane at varying reaction duration

for polyamide chain growth and crosslinking thus producing a thicker and denser polyamide film. By 30 s, the polyamide film had evolved into a structure with pore size of 0.64 nm and effective thickness/porosity of 24.6 μm. MPD continued to diffuse into this relatively loose polyamide film for further polyamide chain growth and crosslinking. As time progressed, the thicker and denser membrane gradually restricted the MPD diffusion through it. Hence, MPD was more likely to collide with the -COCl crosslinking sites in the polyamide film before reaching the reaction zone. As a result, strong membrane pore tightening was observed at 60 s. In spite of this, the membrane porosity was enhanced by the region of thickness growth between 30 and 60 s, which was relatively porous as polyamide chain crosslinking was limited by the MPD diffusion resistance. This explained the plateau of membrane effective thickness/porosity at 30 and 60 s.

By extending the reaction beyond 60 s, the thicker and better crosslinked polyamide film represented significant MPD diffusion barrier. Self-limitation occurred where polyamide chain and film thickness growth became limited as MPD could hardly reach the reaction zone deep in organic solution. In fact, only little MPD could enter the bottom region of polyamide film for polyamide chain crosslinking. Hence, the membrane experienced slight pore tightening and thickness increment only at 90 s. However, the marginal decrease of effective thickness/porosity led to the speculation of mild porosity increase at 90 s. Firstly, the membrane porosity was enhanced by the small region of thickness growth, which was porous with limited polyamide chain crosslinking. Besides, the -COCl crosslinking sites far away from the liquid-liquid interface were highly susceptible to hydrolysis before being reacted by the limited MPD at such prolonged reaction. This left the top region of polyamide film with a relatively porous structure. Therefore, the polyamide film possessed uneven porosity distribution in normal direction to the membrane growth. This non-linear feature of interfacial polymerization was also discovered and highlighted by other researches (Hermans

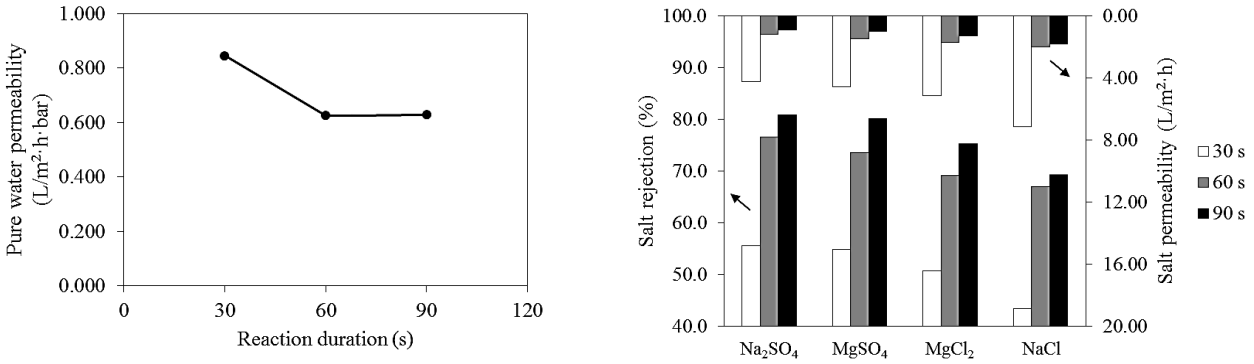

(a) (b)

Fig. 6: Transport properties of TFC membrane at varying reaction duration for (a) pure water (b) inorganic salts.

et al. 2015, Lee et al. 2013).

The membrane temporal evolution plays a pivotal role in impacting the TFC membrane performance. This is indicated by the markedly distinct membrane transport properties in **Figure 6**. From Figure 6 (a), the pure water permeability declined sharply by 26.0 % from 30 to 60 s then stabilized at 90 s. At 30 s, the pure water permeability was high as the polyamide film was loose and thin culminating in low water transport resistance through the polyamide film. However, severe membrane pore tightening and thickness growth from 30 to 60 s combined to limit the water passage across membrane hence drastically reducing the pure water permeability at 60 s. Moving onto 90 s, while the polyamide film continued to densify and grew slightly thicker to restrict water transport, this was offset by the slight increase of membrane porosity and hydrophilicity induced by -COCl hydrolysis. Hence, similar pure water permeability was obtained at 60 and 90 s.

Meanwhile, Figure 6 (b) shows that the salt rejection improved significantly from 30 to 60 s before slightly increased from 60 to 90 s. The continuous salt rejection enhancement was due to gradual membrane pore tightening, which intensified its molecular sieving effect. This was further vindicated as the magnitude of pore size reduction correlated well with the degree of salt rejection increase. With substantial rise of salt rejection and diminished effect of convective salt transport at lower pure water permeability, it was not surprising that salt permeability at 60 s was at least 66.1 % lower compared to 30 s. However, the salt permeability only dropped modestly from 60 to 90 s as this period oversaw little salt rejection improvement with comparable convective salt transport effect under similar pure water permeability.

Salt Separation Mechanism of TFC Membrane

From previous discussion, the salt rejection for every series of TFC membrane was found to be highly dependent on size exclusion effect. However, this could not be the only working salt separation principle as the pore size of every membrane was larger than the size of every hydrated ion in this study as listed in

Table 2. This highlighted the presence of other salt retention mechanism such as Donnan exclusion effect, which separates salt via interaction between ions and fixed electrical charges on membrane (Yaroshchuk 2001). This mechanism is common among the TFC membrane and has been reported by a few studies (Fang et al. 2013, Schaep et al. 1998, Sum et al. 2014).

Table 2. Hydrated Radius of Divalent and Monovalent Ions (Nightingale Jr. 1959)

Ion	Hydrated radius (nm)
Mg^{2+}	0.428
SO_4^{2-}	0.379
Na^+	0.358
Cl^-	0.332

To apprehend Donnan exclusion principle, the charge nature of polyamide film was evaluated by permeation test using salts with single and multiple valence on both cationic and anionic counterparts. The salts typically used are NaCl, Na_2SO_4, $MgCl_2$ and $MgSO_4$ as in this study and also the work of other researches (Fang et al. 2013, Schaep et al. 1998, Sum et al. 2014). From Figure 2 (b), Figure 4 (b) and Figure 6 (b), the relative salt rejection order was always Na_2SO_4 > $MgSO_4$ > $MgCl_2$ > NaCl regardless of membrane synthesis condition. The better rejection of SO_4^{2-} containing salts than Cl^- containing salts suggested the formation of a negatively charged membrane as the coion with higher ionic valence experienced stronger electrostatic repulsion with membrane to enhance Donnan exclusion effect (Fang et al. 2013, Yaroshchuk 2001). The TFC membrane attained negative charges through -COO^- from the dissociation of -COOH that originated from hydrolysis of -COCl in polyamide film.

Nonetheless, to completely describe the relative salt rejection order, size exclusion effect must also be considered where the larger hydrated ion has a better rejection due to stronger steric hindrance by membrane pore. This explained the higher $MgSO_4$ rejection compared to $MgCl_2$ (hydrated SO_4^{2-} ion larger than hydrated Cl^- ion) as well as the higher $MgCl_2$ rejection compared to NaCl (hydrated Mg^{2+} ion larger than hydrated Na^+ ion). However, Na_2SO_4 displayed higher rejection than $MgSO_4$ despite the hydrated Na^+ ion being smaller than the hydrated Mg^{2+} ion. This was ascribed to the masking of membrane anionic electric field by divalent Mg^{2+}, which diminished the Donnan exclusion effect to worsen the rejection of hydrated SO_4^{2-} ion for $MgSO_4$ (Schaep et al. 1998). While similar membrane charge perturbation occurred for $MgCl_2$, the effect was not sufficiently strong to invert the rejection sequence of $MgCl_2$ and NaCl. This was due to lower ionic valence of hydrated Cl^- ion making it less susceptible to the impaired Donnan exclusion effect by Mg^{2+}.

Membrane Selection Criteria for Desalination

In this work, it was clearly shown that membrane preparation condition adjustment has a direct impact on the polyamide film structure, which translates into wide range of membrane transport behaviors. Therefore, proper membrane synthesis condition are required in order

Table 3. Permeability Ratio of TFC Membrane and Corresponding Synthesis Condition

MPD concentration (w/v%)	TMC concentration (w/v%)	Reaction duration (s)	Permeability ratio (bar^{-1})
1	0.10	60	0.175
2	0.10	60	0.313
3	0.10	60	0.673
2	0.05	60	0.288
2	0.15	60	0.201
2	0.10	30	0.119
2	0.10	90	0.346

to produce a TFC membrane with excellent desalination performance. In this context, each membrane synthesis variable can be selected independently based on the membrane performance. However, this method is flawed as it fails to recognize possible interaction between parameters affecting the membrane formation. For instance, high MPD concentration will result in a well-crosslinked polyamide film so long extent of reaction is not necessary to further improve polyamide chain crosslinking.

Instead, the TFC membrane should be analyzed based on the desalination performance criteria, which are high water flux and retention of NaCl, a major component found in typical desalination feed. In other words, one needs to evaluate the selectivity of TFC membrane by comparing the intrinsic transport property of water and NaCl, which is their respective permeability. Mathematically, the membrane selectivity is indicated by the ratio of pure water permeability to NaCl permeability with higher value being preferable as water transport is favored over NaCl transport. The permeability ratio of every membrane in this study is summarized in **Table 3**. The TFC membrane synthesized from 3 w/v% MPD concentration and 0.10 w/v% TMC concentration under 60 s reaction duration achieved the best desalination performance. Its permeability ratio of 0.673 was nearly twice higher than the next best TFC membrane at 0.346. The polyamide film formed at these synthesis condition was very thin but tightly crosslinked and achieved pure water permeability of 0.853 $L/m^2 \cdot h \cdot bar$ with 81.4 % NaCl rejection.

CONCLUSION

In this work, structurally distinct polyamide TFC membranes were successfully synthesized by regulating MPD and TMC monomer concentration as well as reaction duration during interfacial polymerization. It was found that increasing MPD concentration promoted polyamide chain crosslinking during diffusion-limited growth stage to ultimately retard polyamide chain growth. Meanwhile, higher TMC concentration led to a thicker incipient polyamide film that favored polyamide chain growth over

crosslinking during diffusion-limited growth stage. Moreover, longer reaction duration allowed prolonged degree of polyamide chain crosslinking and growth to eventually cause self-limiting polyamide film growth. Generally, water transport was restricted by a thicker membrane obtained under enhanced polyamide chain growth. However, this was overcome by severe -COCl hydrolysis at high TMC concentration and long reaction duration owing to formation of a more porous and hydrophilic polyamide film. Meanwhile, salt rejection correlated well with the membrane pore size that was governed by polyamide chain crosslinking. Nevertheless, the polyamide film achieved salt separation via synergistic effects of size exclusion and Donnan exclusion. In this work, the TFC membrane synthesized at 3 w/v% MPD concentration and 0.10 w/v% TMC concentration under 60 s reaction duration had a very thin but dense morphology that achieved the best desalination performance with pure water permeability of 0.853 $L/m^2 \cdot h \cdot bar$ and 81.4 % NaCl rejection.

ACKNOWLEDGEMENTS

The authors are grateful to the financial support provided by Universiti Sains Malaysia Research University Grant (RUI) (1001/PJKIMIA/814210) and Universiti Sains Malaysia Fellowship Scheme.

REFERENCES

1. Ahmad, A. L., and Ooi, B. S. (2005). Properties–performance of thin film composites membrane: study on trimesoyl chloride content and polymerization time, *J. Membr. Sci.*, *255*, 67.
2. Atherton, J. H. (1994). *Mechanism in two-phase reaction systems: coupled mass transfer and chemical reaction*, in: R.G. Compton, G. Hancock (Eds.), Research in Chemical Kinetics, Elsevier Science B. V., Amsterdam.
3. Bowen, W. R., Mohammad, A. W., and Hilal, N. (1997). Characterisation of nanofiltration membranes for predictive purposes—use of salts, uncharged solutes and atomic force microscopy, *J. Membr. Sci.*, *126*, 91.
4. Bowen, W. R., and Mukhtar, H. (1996). Characterisation and prediction of separation performance of nanofiltration membranes, *J. Membr. Sci.*, *112*, 263.
5. Cadotte, J. E., and Rozelle, L. T. (1972). *In situ-Formed Condensation Polymers for Reverse Osmosis Membranes*, North Star Research and Development Institute, U.S.A.
6. Chai, G. Y., and Krantz, W. B. (1994). Formation and characterization of polyamide membranes via interfacial polymerization, *J. Membr. Sci.*, *93*, 175.
7. El-Aassar, A. M. A. (2012). Polyamide thin film composite membranes using interfacial polymerization: synthesis, characterization and reverse osmosis performance for water desalination, *Aust. J. Basic Appl. Sci.*, *6*, 382.
8. Fang, W., Shi, L., and Wang, R. (2013). Interfacially polymerized composite nanofiltration hollow fiber membranes for low-pressure water softening, *J. Membr. Sci.*, *430*, 129.
9. Fick, A. (1855). V. On liquid diffusion, *Lond. Edinb. Dubl. Phil. Mag.*, *10*, 30.

10. Freger, V. (2005). Kinetics of film formation by interfacial polycondensation, *Langmuir*, *21*, 1884.
11. Hermans, S., Bernstein, R., Volodin, A., and Vankelecom, I. F. J. (2015). Study of synthesis parameters and active layer morphology of interfacially polymerized polyamide–polysulfone membranes, *React. Funct. Polym.*, *86*, 199.
12. Lee, J., Hill, A., and Kentish, S. (2013). Formation of a thick aromatic polyamide membrane by interfacial polymerisation, *Sep. Purif. Technol.*, *104*, 276.
13. Nightingale Jr., E. R. (1959). Phenomenological theory of ion solvation. Effective radii of hydrated ions, *J. Phys. Chem.*, *63*, 1381.
14. Petersen, R. J. (1993). Composite reverse osmosis and nanofiltration membranes, *J. Membr. Sci.*, *83*, 81.
15. Roh, I. J., Greenberg, A. R., and Khare, V. P. (2006). Synthesis and characterization of interfacially polymerized polyamide thin films, *Desalination*, *191*, 279.
16. Rudin, A., and Choi, P. (2012). *The Elements of Polymer Science & Engineering*, Academic Press, Waltham.
17. Schaep, J., Van der Bruggen, B., Vandecasteele, C., and Wilms, D. (1998). Influence of ion size and charge in nanofiltration, *Sep. Purif. Technol.*, *14*, 155.
18. Song, Y., Sun, P., Henry, L. L., and Sun, B. (2005). Mechanisms of structure and performance controlled thin film composite membrane formation via interfacial polymerization process, *J. Membr. Sci.*, *251*, 67.
19. Soroush, A., Barzin, J., Barikani, M., and Fathizadeh, M. (2012). Interfacially polymerized polyamide thin film composite membranes: Preparation, characterization and performance evaluation, *Desalination*, *287*, 310.
20. Sum, J. Y., Ahmad, A. L., and Ooi, B. S. (2014). Synthesis of thin film composite membrane using mixed dendritic poly (amidoamine) and void filling piperazine monomers, *J. Membr. Sci.*, *466*, 183.
21. Tomaschke, J. E. (2000). Interfacial composite membranes, *III/Membr. Prep.*, 3319.
22. Yaroshchuk, A. E. (2001). Non-steric mechanisms of nanofiltration: superposition of Donnan and dielectric exclusion, *Sep. Purif. Technol.*, *22*, 143.